Conference Proceedings of the Society for Experimental Mechanics Series

Matt Allen · Randall L. Mayes · Daniel Rixen *Editors*

Dynamics of Coupled Structures, Volume 4

Proceedings of the 34th IMAC, A Conference and Exposition on Structural Dynamics 2016

SEM

Springer

Conference Proceedings of the Society for Experimental Mechanics Series

Series Editor
Kristin B. Zimmerman, Ph.D.
Society for Experimental Mechanics, Inc.,
Bethel, CT, USA

More information about this series at http://www.springer.com/series/8922

Matt Allen • Randall L. Mayes • Daniel Rixen
Editors

Dynamics of Coupled Structures, Volume 4

Proceedings of the 34th IMAC, A Conference and Exposition on Structural Dynamics 2016

Springer

Editors
Matt Allen
Engineering Physics Department
University of Wisconsin Madison
Madison, WI, USA

Randall L. Mayes
Sandia National Laboratories
Albuquerque, NM, USA

Daniel Rixen
Lehrstuhl für Angewandte Mechanik
Technische Universitat München
Garching, Bayern, Germany

ISSN 2191-5644 ISSN 2191-5652 (electronic)
Conference Proceedings of the Society for Experimental Mechanics Series
ISBN 978-3-319-29762-0 ISBN 978-3-319-29763-7 (eBook)
DOI 10.1007/978-3-319-29763-7

Library of Congress Control Number: 2014932412

Printed on acid-free paper

This Springer imprint is published by Springer Nature
The registered company is Springer International Publishing AG Switzerland

Preface

Dynamics of Coupled Structures represents one of ten volumes of technical papers presented at the 34th IMAC, A Conference and Exposition on Structural Dynamics, organized by the Society for Experimental Mechanics and held in Orlando, Florida, January 25–28, 2016. The full proceedings also include volumes on nonlinear dynamics; dynamics of civil structures; model validation and uncertainty quantification; sensors and instrumentation; special topics in structural dynamics; structural health monitoring, damage detection, and mechatronics; rotating machinery, hybrid test methods, vibro-acoustics, and laser vibrometry; and shock and vibration, aircraft/aerospace, energy harvesting, acoustics and optics, and topics in modal analysis and testing.

Each collection presents early findings from experimental and computational investigations on an important area within structural dynamics. Coupled structures or substructuring is one of these areas.

Substructuring is a general paradigm in engineering dynamics where a complicated system is analyzed by considering the dynamic interactions between subcomponents. In numerical simulations, substructuring allows one to reduce the complexity of parts of the system in order to construct a computationally efficient model of the assembled system. A subcomponent model can also be derived experimentally, allowing one to predict the dynamic behavior of an assembly by combining experimentally and/or analytically derived models. This can be advantageous for subcomponents that are expensive or difficult to model analytically. Substructuring can also be used to couple numerical simulation with real-time testing of components. Such approaches are known as hardware-in-the-loop or hybrid testing.

Whether experimental or numerical, all substructuring approaches have a common basis, namely, the equilibrium of the substructures under the action of the applied and interface forces and the compatibility of displacements at the interfaces of the subcomponents. Experimental substructuring requires special care in the way the measurements are obtained and processed in order to assure that measurement inaccuracies and noise do not invalidate the results. In numerical approaches, the fundamental quest is the efficient computation of reduced order models describing the substructure's dynamic motion. For hardware-in-the-loop applications, difficulties include the fast computation of the numerical components and the proper sensing and actuation of the hardware component. Recent advances in experimental techniques, sensor/actuator technologies, novel numerical methods, and parallel computing have rekindled interest in substructuring in recent years leading to new insights and improved experimental and analytical techniques.

The organizers would like to thank the authors, presenters, session organizers, and session chairs for their participation in this track.

Madison, WI, USA	Matt Allen
Albuquerque, NM, USA	Randall L. Mayes
Garching, Bayern, Germany	Daniel Rixen

Contents

Chapter 1
Verification of Experimental Component Mode Synthesis in the Sierra Analysis Framework

Brian C. Owens and Randall L. Mayes

Abstract Experimental component mode synthesis (CMS) seeks to measure the fundamental modes of vibration of a substructure and develop a structural dynamics model of an as-built structural component through modal testing. Experimental CMS has the potential to circumvent laborious and costly substructure model development and calibration in lieu of a structural dynamics model obtained directly from experimental measurements. Previous efforts of interfacing an experimental CMS model with a production finite element code proved cumbersome. Recently an improved "Craig-Mayes" approach casts an experimental CMS model in the familiar Craig-Bampton form. This form is easily understood by analysts and more readily interfaced with non-trivial, discrete finite element models. The approach/work-flow for interfacing an experimental Craig-Mayes CMS model with the Sierra analysis framework is discussed and the procedure is demonstrated on a verification problem.

Keywords Component mode synthesis • Craig-Bampton • Substructure • Sierra • Finite elements

Nomenclature

CMS	Component mode synthesis
FE	Finite element(s)
M	Mass matrix
TS	Transmission simulator

1.1 Introduction

The concept of experimental component mode synthesis (CMS) seeks to measure the fundamental modes of vibration of a substructure and develop a structural dynamics model of a component or subsystem which may be inserted into an analytical model of a higher-level system. Strengths of experimental CMS allow for one to circumvent laborious and costly substructure model development and calibration in lieu of a structural dynamics model obtained directly from experimental measurements. Furthermore, experimental CMS allows for a better modelling capability of as-built structural components.

This work will interface an experimentally derived "Craig-Bampton" like substructure with a discrete finite element model within Sandia National Laboratories Sierra analysis framework [1, 2]. A previously developed transmission simulation approach is employed to match interface locations with a discrete system level finite element model. Previous efforts will be discussed and strengths of the current approach in streamlining the use of experimentally derived substructures will be highlighted. This approach will be discussed and verification exercises will be presented.

Sandia National Laboratories is a multi-program laboratory managed and operated by Sandia Corporation, a wholly owned subsidiary of Lockheed Martin Corporation, for the U.S. Department of Energy National Nuclear Security Administration under Contract DE-AC04-94AL85000.

B.C. Owens (✉) • R.L. Mayes
Sandia National Laboratories, P.O. Box 5800 – MS0346, Albuquerque, NM 87185, USA
e-mail: bcowens@sandia.gov; rlmayes@sandia.gov

M. Allen et al. (eds.), *Dynamics of Coupled Structures, Volume 4*, Conference Proceedings of the Society for Experimental Mechanics Series, DOI 10.1007/978-3-319-29763-7_1

1.2 Craig-Mayes Experimental Sub-Structuring Method

The Craig-Mayes experimental dynamic sub-structuring method improves upon previous experimental sub-structuring methods by representing the substructure system matrices (mass, stiffness, and damping) in a Craig-Bampton [3] like form. This form contains structural matrices with generalized/modal and interface degrees of freedom. This approach uses a transmission simulator to model the interface of the sub-structure to the remainder of the system. The transmission simulator approach requires an accurate discrete finite element model of the transmission simulator/fixture to accurately recover the interface degrees of freedom in an experimental substructure. The Craig-Mayes experimental sub-structuring method and transmission simulator approach are discussed in references [4, 5].

1.3 Interface of Experimental CMS Model to Sierra

Previous efforts of coupling experimental CMS models within the Sierra framework employed multi-point constraints and a non-Craig-Mayes CMS representation. This approach proved overly cumbersome for all but the simplest model configurations, and was prone to numerical conditioning issues. The Craig-Mayes format provides a readily realizable interface to a high fidelity structural dynamics model with an interface similar to CMS or “super element” model derived purely from analytical methods. The experimental CMS model is typically provided by experimentalists as a collection of Craig-Bampton like mass, stiffness, and damping matrices [4]. Note that the damping matrix is not required to define a baseline experimental CMS model, but is readily available from experimental measurements.

The Craig-Bampton like matrices are $p \times p$ in dimension, such that $p = m + n$. Here, m is the number of modes retained in the CMS reduction, and n is the number of interface degrees of freedom in the CMS model. The required form of these equations is shown in Eq. (1.1). Note that the form of the mass matrix is shown, but identical forms are required for the stiffness and damping matrices. These matrices are symmetrical in nature. $\hat{M}$ defines couplings between the generalized (modal) degrees of freedom in the CMS model (this matrix should be diagonal in nature), $\overline{M}$ defines couplings between the interface degrees of freedom, and $\widetilde{M}$ defines the couplings between generalized and interface degrees of freedom.

$$M_{CMS} = \begin{bmatrix} \hat{M}_{m\times m} & \widetilde{M}_{m\times n} \\ \widetilde{M}^{T}_{m\times n} & \overline{M}_{n\times n} \end{bmatrix} \tag{1.1}$$

An $r \times 3$ coordinate array is also required that defines the coordinates of the r interface points. In addition to interface point coordinates an $n \times 1$ map array is required that specifies the “local” degrees of freedom of the interface degrees of freedom. The order of this array should be consistent with the ordering of the coordinate array.

In summary, the following data is required to accompany an experimentally derived CMS model:

- Number of modes retained in the CMS reduction (m)
- Number of interface degrees of freedom (n)
- Interface point coordinate array
- CMS mass matrix
- CMS stiffness matrix
- Interface degree of freedom map array
- CMS damping matrix (optional)

This information can be provided to the MATLAB based “CMS Toolkit” to create a Sierra super element of the experimental CMS model. The CMS toolkit creates two files. First, an Exodus finite element mesh is created defining the geometry of the super element. This includes the coordinates of the interface nodes for the n-node super element. Next, the formulation of this super element (mass, stiffness, and damping) are characterized in a NetCDF binary file. The super element Exodus file is inserted into a discrete finite element model using GJOIN [6] or a similar mesh joining utility. From here, the super element NetCDF file is referenced in a Sierra input deck and subsequent modal, vibration, or transient analysis accounts for the coupling between the discrete finite element model and the experimentally derived Craig-Mayes substructure. This workflow is depicted in Fig. 1.1.

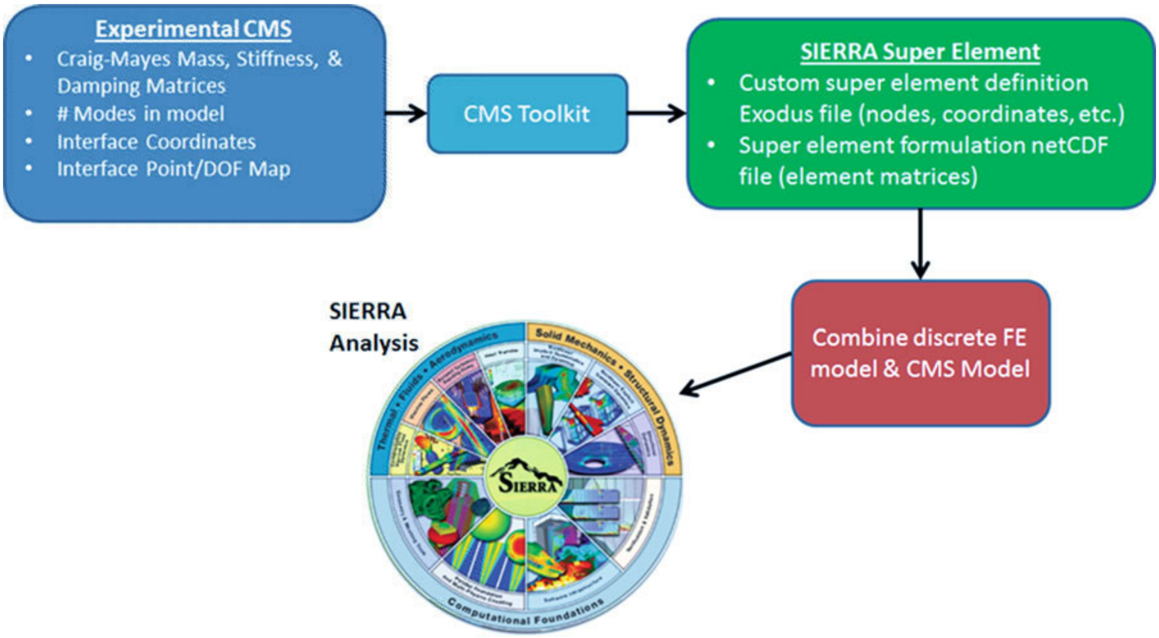

Fig. 1.1 Workflow for interfacing an experimentally derived CMS model in Sierra analysis

1.4 Demonstration

This section presents a demonstration of the aforementioned process for interfacing an experimentally derived Craig-Mayes substructure to a discrete finite element modal for Sierra-SD analysis. First the model/test configuration is described followed by results of the exercise.

1.4.1 Configuration

A 2-D simple beam configuration documented in reference [4] was considered for a proof of concept analysis for interfacing an experimentally derived CMS substructure model with Sierra-SD analysis. The configuration is shown in Fig. 1.2. Two beams are connected together over a specified region of overlap. The left beam is to be modeled by finite elements, whereas the dynamics of the right beam are measured experimentally and an experimental CMS model is derived. This is done using a "transmission simulator" shown as "TS Beam" in Fig. 1.2. Details of the transmission simulator are elaborated on in references [4, 5]. The transmission simulator essentially allows one to generate interface degree of freedom responses at discrete locations from those measured from a modal test. This is a very convenient means for interfacing an experimentally derived CMS model to discrete points of a finite element model.

Note that there are five nodes in the overlap between the left finite element beam and the right experimental CMS beam. Thus, the transmission simulator approach was used to derive an experimental CMS model with five interface points (coincident with the finite element nodes). Each interface point had 3 degrees of freedom (axial translation, bending translation, and rotation). Therefore, a total of 15 interface degrees of freedom exist in the model. Three modes were retained in the CMS reduction. This resulted in CMS mass, stiffness, and damping matrices that had dimension of 18×18.

1.4.2 Results

The Craig-Mayes substructure model of the beam was interfaced to the discrete "FE Beam" model in Sierra-SD described in Sect. 1.2. Results show good agreement between the "truth model" described in reference [4] and the Sierra-SD implementation. Table 1.1 presents a comparison of modal frequencies. The first five modes have 1 % error or less and

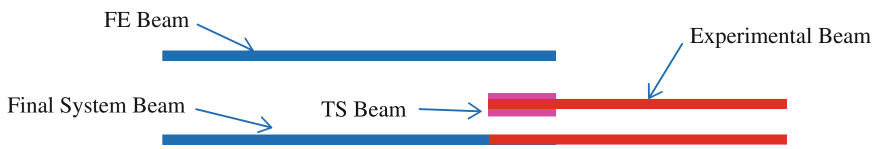

Fig. 1.2 2D beam configuration [4]

Table 1.1 Comparison of Sierra-SD sub-structured modal frequency vs. truth frequency

Truth frequency (Hz) [4]	Sierra-SD sub-structured frequency (Hz)	Error (%)
212.0	210.4	−0.7
574.6	568.6	−1.0
1121.0	1132.0	1.0
1867.3	1863.9	−0.2
2750.2	2767.6	0.6
3341.7	3383.9	1.3
3949.6	4003.2	1.4
5115.9	5105.0	−0.2
5965.5	5945.8	−0.3

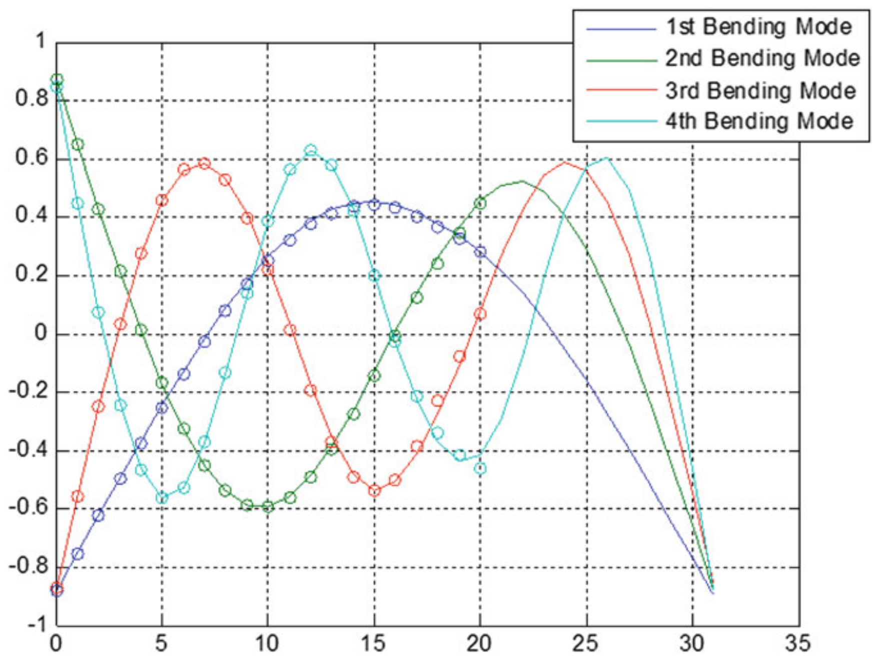

Fig. 1.3 Comparison of "truth" and Sierra-SD sub-structured lower bending mode shapes (*solid line* = truth model, *circle* = sub-structured model)

the 6th–9th modes have at most 1.4 % error. Bending mode shape comparisons of a discrete finite element model of the entire system and those of the discrete "FE beam" coupled with the Craig-Mayes experimental beam are shown in Figs. 1.3 and 1.4. Solid lines represent the finite element results of the complete system while markers represent the mode shape of the discrete left beam coupled with the Craig-Mayes right beam. Overall, good agreement is seen between the "truth" FEM mode shapes and those of the discrete finite element model of the left beam coupled to the Craig-Mayes substructure of the right beam. Some differences are apparent for the 4th–7th bending mode shapes in the vicinity of the interface to the Craig-Mayes substructure. This may be due to some artifacts of the transmission simulator approach providing an increased stiffening effect at this location.

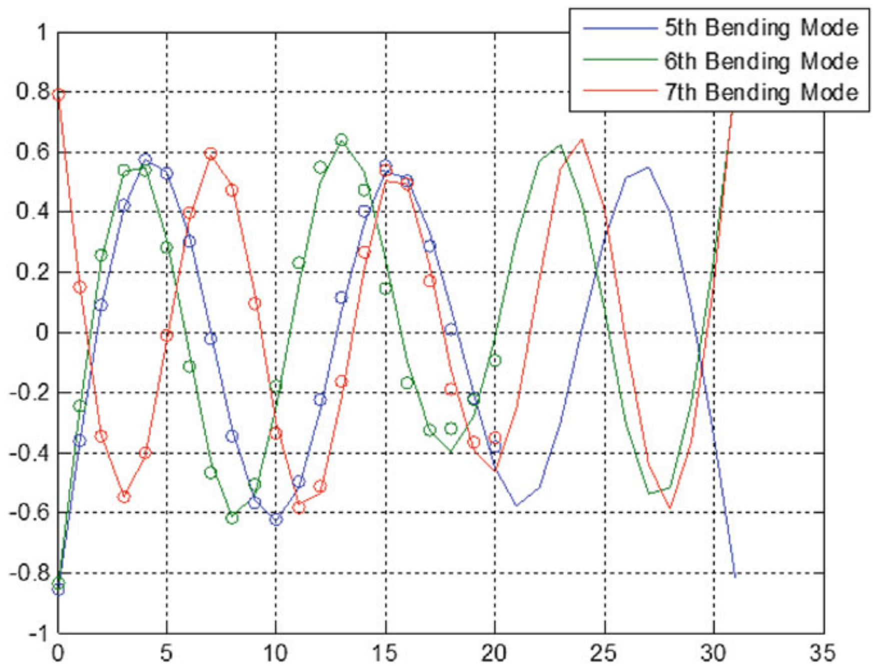

Fig. 1.4 Comparison of "truth" and Sierra-SD sub-structured higher bending mode shapes (*solid line* = truth model, *circle* = sub-structured model)

1.5 Conclusions

This paper has presented the motivation for using experimentally derived substructures within the Sierra analysis framework. The Craig-Mayes sub-structuring approach allows for a straightforward interface of an experimental CMS model with a discrete finite element model by using a representation similar to the Craig-Bampton CMS approach. This allows for the experimental CMS model to be treated virtually the same way as a numerically derived Craig-Bampton "super element", although the experimental model may be prone to some numerical conditioning issues as a result of flaws in measurement data and mathematical operations being performed on that data. The work-flow of interfacing a Craig-Mayes model with the Sierra analysis framework was discussed and the process was demonstrated successfully on a proof-of-concept application.

Future work will consider more complicated substructures. This may include sub-structures generated from actual experimental data or substructures derived from "virtual" modal testing with the Sierra-SD analysis software. The concept of virtual modal testing allows for more idealized accelerometer data to be considered within the general process of an experimental sub-structuring method while allowing control of the imperfections in the test data through the introduction of measurement noise or other flaws.

References

1. Reese, G., Bhardwaj, M., Walsh, T.: Sierra Structural Dynamics-Theory Manual. Sandia National Laboratories, Albuquerque (2014)
2. Sierra Structural Dynamics Development Team: Sierra Structural Dynamics-User's Notes. Sandia National Laboratories, Albuquerque (2014)
3. Craig, R.R., Bampton, M.C.: Coupling of substructures for dynamic analysis. AIAA J. **6**(7), 1313–1319 (1968)
4. Mayes, R.L.: A Craig-Bampton experimental dynamic substructure using the transmission simulator method. In: Proceedings of the 32nd International Modal Analysis Conference, Orlando, February 2015
5. Allen, M.S., Kammer, D.C., Mayes, R.L.: Experimental based substructuring using a Craig-Bampton transmission simulator model. In: Proceedings of the 32nd International Modal Analysis Conference, Orlando, February 2014
6. Sjaardema, G.D.: GJOIN: a program for merging two or more GENESIS databases, SAND92-2290 (1992)

Chapter 2
Multi-DoF Interface Synchronization of Real-Time-Hybrid-Tests Using a Recursive-Least-Squares Adaption Law: A Numerical Evaluation

Andreas Bartl, Johannes Mayet, Morteza Karamooz Mahdiabadi, and Daniel J. Rixen

Abstract Cyber Physical Testing or Real Time Hybrid Testing is a Hardware-In-The-Loop approach allowing for tests of structural components of complex machines with realistic boundary conditions by coupling virtual components. The need to actuate the physical interface makes the tests on structural systems challenging. In order to deal with stability and accuracy issues, we propose the use of an Adaptive Feed-Forward Cancellation approach with a Recursive Least Squares (RLS) adaption law for interface synchronization of harmonically excited systems. The interface forces are generated from multiple harmonic components of the excitation force. A RLS adaption law sets the amplitudes and phases of the harmonic interface force components and minimizes the interface gap. One major practical advantage of using a RLS adaption law is that only one forgetting factor has to be chosen compared to other adaption algorithms with various tuning parameters. As a consequence, it is possible to test systems with multiple interface DoF. In order to illustrate the performance and robustness of the proposed testing algorithm, the contribution includes a numerical investigation on a lumped mass system.

Keywords Hybrid testing • Hardware-in-the-loop • Real-time substructuring • Interface synchronization • Recursive least squares

2.1 Introduction

Real Time Hybrid Testing, Cyber Physical Testing or Hardware-in-the-Loop for structural systems is a testing approach connecting experimental test rigs (experimental component) with simulation models (virtual component) in a real time test (see Figs. 2.1 and 2.2). In contrast of testing the experimental component by applying fictitious load cases, realistic boundary conditions are provided in these test procedures. The approach is always valuable were neither full experimental tests nor full simulations are applicable. Real Time Hybrid Testing was applied in engineering of earthquake save civil structures in [3, 12, 17]. A testing example on a full wind turbine nacelle is presented in [6] and an automotive application is given in [18].

The objective of the interface synchronization control in Real Time Hybrid Testing (RTHT) is to satisfy equilibrium and compatibility constraints within the desired frequency range. Consider for example structural applications with commonly low damping of the overall system. Controlling a system with poles close to the imaginary axis can cause instability of the real time test due to small control errors and inaccuracies in measurement or actuation. The problem of interface synchronization is closely linked to actual compensation methods. The performance of actuator compensation methods is compared in [5]. The authors of [15, 21] present frameworks for the development of RTHT controllers. A Linear-Quadratic-Regulator controller framework is presented in [22]. In the contribution [7] the Real Time Hybrid Testing problem is analyzed with conventional control theory. As in many applications the dynamics of the experimental substructures are unknown, Model Reference Adaptive Control (MRAC) is proposed as a control strategy in [19, 23]. A widely used approach is based on polynomial forward prediction used in [8, 12] for compensation of the actuator dynamics. The authors of [24] extend this approach by gain and phase estimation. More recently neuronal network feedforward compensation for the use in Real Time Hybrid Testing were proposed in [16]. Model Predictive Control is proposed as a control strategy for RTHT in [20].

In [1] we presented a adaptive feedforward algorithm with a harmonic regressor (see e.g. [2, 4, 10]) applied to RTHT. The adaption is based on a gradient algorithm. This approach is closely linked to fxLMS Algorithm as presented in [14]. However, in case of multiple DoF interfaces the choice of the adaption gain matrix, which defines the stability of the algorithm, is getting impractical. The entries of the adaption gain matrix can vary within several orders of magnitude and wrong choices may cause instability of the test. Therefore, we propose in this contribution an adaptive feedforward filter with harmonic

A. Bartl (✉) • J. Mayet • M.K. Mahdiabadi • D.J. Rixen
Technical University of Munich, Boltzmannstraße 15, D-85748 Garching, Germany
e-mail: andreas.bartl@tum.de

M. Allen et al. (eds.), *Dynamics of Coupled Structures, Volume 4*, Conference Proceedings of the Society for Experimental Mechanics Series, DOI 10.1007/978-3-319-29763-7_2

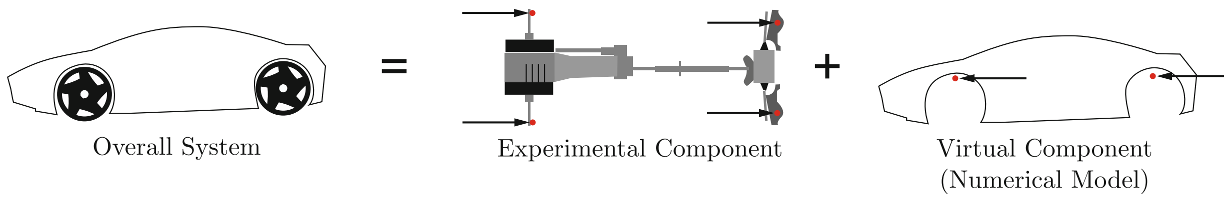

Fig. 2.1 The overall system is split into a virtual and an experimental component

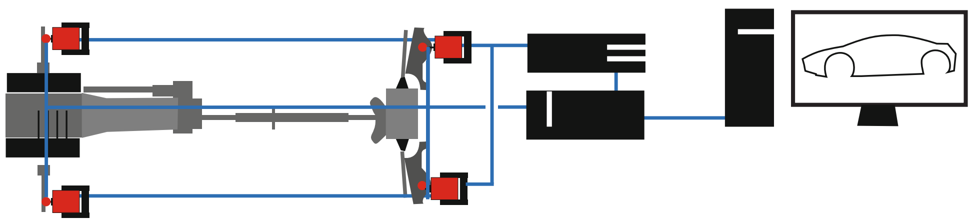

Fig. 2.2 The test rig is coupled with sensors and actuators to the virtual component running on a real time computer

regressor based on a Recursive Least Squares (RLS) adaption law with only a single tuning parameter. The fact that the user has only to choose one tuning parameter makes the suggested approach applicable to carry out various tests on systems with a multi DoF interface.

2.2 Hybrid Testing Problem Formulation

The objective of the RTHT control is to satisfy compatibility (Eq. (2.1)) and equilibrium (Eq. (2.2)) constraints between virtual and experimental components. The Boolean matrices $\boldsymbol{G}_V$ and $\boldsymbol{G}_E$ are selecting the interface forces and displacements (see [9] for details). $\boldsymbol{y}_{b,V}$ and $\boldsymbol{y}_{b,E}$ are the interface displacement vectors. The interface gap is denoted as $\boldsymbol{e}$. $\boldsymbol{f}_{b,V}$ and $\boldsymbol{f}_{b,E}$ are the interface force vectors

$$\boldsymbol{G}_V\boldsymbol{u} - \boldsymbol{G}_E\boldsymbol{u} = \boldsymbol{y}_{b,V} - \boldsymbol{y}_{b,E} = \boldsymbol{e} = \boldsymbol{0} \tag{2.1}$$

$$\boldsymbol{G}_V\boldsymbol{f}_{b,V} + \boldsymbol{G}_E\boldsymbol{f}_{b,E} = \boldsymbol{0} \tag{2.2}$$

In principal two distinctive ways for setting up an control scheme do exist. One possibility is to define the interface displacements as compatible and controlling the interface forces in order to achieve equilibrium. In contrast one can define the interface forces as forces with equal magnitude and opposite sign, controlling the interface gap. In this contribution, we use the latter one, which is comparable to the to the dual formulation in substructuring (see [9] for details). In practice, this foregoing is absolutely meaningful since one will end up with forces as controller setpoint rather than gaps which would necessarily require inner-loop actuator control algorithms. The applied forces $\boldsymbol{\lambda}$ are subsequently measured and applied to the virtual subcomponent with opposite sign. The dynamics of both components are given by Eq. (2.3).

$$\begin{bmatrix} \boldsymbol{M}_V & \boldsymbol{0} \\ \boldsymbol{0} & \boldsymbol{M}_E \end{bmatrix} \begin{bmatrix} \ddot{\boldsymbol{u}}_V \\ \ddot{\boldsymbol{u}}_E \end{bmatrix} + \begin{bmatrix} \boldsymbol{D}_V & \boldsymbol{0} \\ \boldsymbol{0} & \boldsymbol{D}_E \end{bmatrix} \begin{bmatrix} \dot{\boldsymbol{u}}_V \\ \dot{\boldsymbol{u}}_E \end{bmatrix} + \begin{bmatrix} \boldsymbol{K}_V & \boldsymbol{0} \\ \boldsymbol{0} & \boldsymbol{K}_E \end{bmatrix} \begin{bmatrix} \boldsymbol{u}_V \\ \boldsymbol{u}_E \end{bmatrix} + \begin{bmatrix} \boldsymbol{G}_V^T \\ -\boldsymbol{G}_E^T \end{bmatrix} \boldsymbol{\lambda} = \begin{bmatrix} \boldsymbol{f}_V \\ \boldsymbol{f}_E \end{bmatrix} \tag{2.3}$$

The objective of an interface synchronization controller will be to apply $\boldsymbol{\lambda}$ such that the interface gap $\boldsymbol{e}$ is closed. The assumptions of the control strategy are an harmonic excitation and steady-state system behaviour. The block diagram of the overall control system is given in Fig. 2.3. Before deriving the algorithm the hybrid testing problem is reformulated such that it can be used for an adaptive feedforward compensator in this section. The corresponding state space formulations are given in Eqs. (2.4) and (2.5).

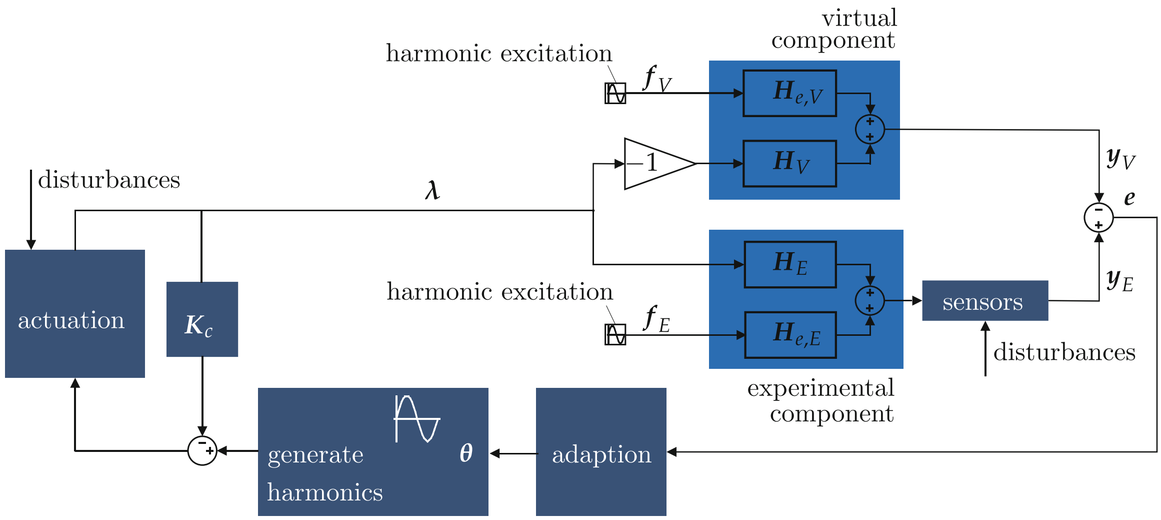

Fig. 2.3 The block diagram shows the hybrid test with adaptive feedforward compensation. Harmonic excitation on both the experimental and virtual component are possible. The actuator is exciting the experimental and contrariwise the virtual component in the present of real and virtual harmonic excitations. The controller adapts phase and gain of the harmonic inputs to the actuator such that the interface gap $\boldsymbol{e}$ is closed. (adapted from [1])

$$\begin{aligned}
\dot{\boldsymbol{x}}_V &= \underbrace{\begin{bmatrix} \mathbf{0} & \boldsymbol{I} \\ -\boldsymbol{M}_V^{-1}\boldsymbol{K}_V & -\boldsymbol{M}_V^{-1}\boldsymbol{D}_V \end{bmatrix}}_{\boldsymbol{A}_V} \boldsymbol{x}_V + \underbrace{\begin{bmatrix} \mathbf{0} \\ \boldsymbol{M}_V^{-1}\boldsymbol{G}_V^T \end{bmatrix}}_{\boldsymbol{B}_V} \boldsymbol{\lambda} + \underbrace{\begin{bmatrix} \mathbf{0} \\ \boldsymbol{M}_V^{-1} \end{bmatrix}}_{\boldsymbol{E}_V} \boldsymbol{f}_V \\
\boldsymbol{y}_V &= \boldsymbol{G}_V \boldsymbol{u}_V = \underbrace{\begin{bmatrix} \boldsymbol{G}_V & \mathbf{0} \end{bmatrix}}_{\boldsymbol{C}_V} \boldsymbol{x}_V
\end{aligned} \tag{2.4}$$

$$\begin{aligned}
\dot{\boldsymbol{x}}_E &= \underbrace{\begin{bmatrix} \mathbf{0} & \boldsymbol{I} \\ -\boldsymbol{M}_E^{-1}\boldsymbol{K}_E & -\boldsymbol{M}_E^{-1}\boldsymbol{D}_E \end{bmatrix}}_{\boldsymbol{A}_E} \boldsymbol{x}_E - \underbrace{\begin{bmatrix} \mathbf{0} \\ \boldsymbol{M}_E^{-1}\boldsymbol{G}_E^T \end{bmatrix}}_{\boldsymbol{B}_E} \boldsymbol{\lambda} + \underbrace{\begin{bmatrix} \mathbf{0} \\ \boldsymbol{M}_E^{-1} \end{bmatrix}}_{\boldsymbol{E}_E} \boldsymbol{f}_E \\
\boldsymbol{y}_E &= \boldsymbol{G}_E \boldsymbol{u}_E = \underbrace{\begin{bmatrix} \boldsymbol{G}_E & \mathbf{0} \end{bmatrix}}_{\boldsymbol{C}_E} \boldsymbol{x}_E
\end{aligned} \tag{2.5}$$

The interface responses can be written as

$$\boldsymbol{y}_V = \underbrace{\int_{t_0}^{t} \boldsymbol{C}_V e^{\boldsymbol{A}_V(t-\tau)} \boldsymbol{B}_V \boldsymbol{\lambda}\, \mathrm{d}\tau}_{\substack{\text{contribution of interface excitation} \\ \text{with transfer function } \boldsymbol{H}_V(j\omega)}} + \underbrace{\int_{t_0}^{t} \boldsymbol{C}_V e^{\boldsymbol{A}_V(t-\tau)} \boldsymbol{E}_V \boldsymbol{f}_V \, \mathrm{d}\tau}_{\text{contribution of external excitation}} + \underbrace{\boldsymbol{C}_V e^{\boldsymbol{A}_V(t-\tau)} \boldsymbol{x}_V(t_0)}_{\text{contribution of initial conditions}} \tag{2.6}$$

$$\boldsymbol{y}_E = \underbrace{\int_{t_0}^{t} \boldsymbol{C}_E e^{\boldsymbol{A}_E(t-\tau)} \boldsymbol{B}_E \boldsymbol{\lambda}\, \mathrm{d}\tau}_{\substack{\text{contribution of interface excitation} \\ \text{with transfer function } \boldsymbol{H}_E(j\omega)}} + \underbrace{\int_{t_0}^{t} \boldsymbol{C}_E e^{\boldsymbol{A}_E(t-\tau)} \boldsymbol{E}_E \boldsymbol{f}_E \, \mathrm{d}\tau}_{\text{contribution of excitation}} + \underbrace{\boldsymbol{C}_E e^{\boldsymbol{A}_E(t-\tau)} \boldsymbol{x}_E(t_0)}_{\text{contribution of initial conditions}} \tag{2.7}$$

Assuming harmonic excitations and steady state behavior, the contribution of initial conditions are neglected. The interface forces can be expressed as a combination of harmonic functions:

$$\begin{aligned}
\boldsymbol{\lambda} &= \sum_{i=1}^{m} \boldsymbol{W}_i(t) \boldsymbol{\theta}_i \\
\boldsymbol{W}_i(t) &= \begin{bmatrix} \boldsymbol{I}_{nn} \cos(\alpha_i) & \boldsymbol{I}_{nn} \sin(\alpha_i) \end{bmatrix} \quad \text{with} \quad \boldsymbol{W}_i \in \mathbb{R}^{n \times 2n}
\end{aligned} \tag{2.8}$$

In Eq. (2.8) the regressor matrix $\boldsymbol{W}_i(t)$ contains the amplitudes for the cosine and sine part of the interface forces and thus the phase angle $\alpha_i = \int_0^t \omega_i(t)\mathrm{d}t$ and frequency $\omega_i(t)$, which are allowed to vary slowly. The important parameter vector $\boldsymbol{\theta}_i$ defines the phases and amplitudes of the interface forces. Since we assume steady state behavior $\boldsymbol{y}_V$ and $\boldsymbol{y}_E$ can now be rewritten as

$$\boldsymbol{y}_V = \sum_{i=1}^{m} \underbrace{\boldsymbol{W}_i(t)\boldsymbol{P}_{V,i}\boldsymbol{\theta}_i}_{\substack{\text{influence} \\ \text{interfaceforces}}} + \underbrace{\boldsymbol{W}_i(t)\boldsymbol{\pi}_{V,i}}_{\substack{\text{influence external} \\ \text{excitation (disturbance)}}} = \boldsymbol{W}(t)\boldsymbol{P}_V\boldsymbol{\theta} + \sum_{i=1}^{m} \boldsymbol{W}_i(t)\boldsymbol{\pi}_{V,i} \tag{2.9}$$

$$\boldsymbol{y}_E = \sum_{i=1}^{m} \underbrace{\boldsymbol{W}_i(t)\boldsymbol{P}_{E,i}\boldsymbol{\theta}_i}_{\substack{\text{influence} \\ \text{interface forces}}} + \underbrace{\boldsymbol{W}_i(t)\boldsymbol{\pi}_{E,i}}_{\substack{\text{influence external} \\ \text{excitation (disturbance)}}} = \boldsymbol{W}(t)\boldsymbol{P}_E\boldsymbol{\theta} + \sum_{i=1}^{m} \boldsymbol{W}_i(t)\boldsymbol{\pi}_{E,i}, \tag{2.10}$$

where the matrices $\boldsymbol{P}_{V,i}$ and $\boldsymbol{P}_{E,i}$ are created using transfer function $\boldsymbol{H}_V(j\omega_1)$ and $\boldsymbol{H}_E(j\omega_1)$ respectively (see Fig. 2.3 and Eqs. (2.11) and (2.12)). These matrices basically apply a phase shift and gain to the parameter vector $\boldsymbol{\theta}$. The vectors $\boldsymbol{\pi}_{V,i}$ and $\boldsymbol{\pi}_{E,i}$ define phase and amplitude of the contributions of the external forces to the interface displacements.

$$\boldsymbol{P}_{V,i} = \begin{bmatrix} Re(\boldsymbol{H}_V(j\omega_i)) & Im(\boldsymbol{H}_V(j\omega_i)) \\ -Im(\boldsymbol{H}_V(j\omega_i)) & Re(\boldsymbol{H}_V(j\omega_i)) \end{bmatrix} = \begin{bmatrix} \boldsymbol{P}_{R,V,i} & \boldsymbol{P}_{I,V,i} \\ -\boldsymbol{P}_{I,V,i} & \boldsymbol{P}_{R,V,i} \end{bmatrix} \quad \text{with} \quad \boldsymbol{P}_{V,i} \in \mathbb{R}^{2n\times 2n} \tag{2.11}$$

$$\boldsymbol{P}_{E,i} = \begin{bmatrix} Re(\boldsymbol{H}_E(j\omega_i)) & Im(\boldsymbol{H}_E(j\omega_i)) \\ -Im(\boldsymbol{H}_E(j\omega_i)) & Re(\boldsymbol{H}_E(j\omega_i)) \end{bmatrix} = \begin{bmatrix} \boldsymbol{P}_{R,E,i} & \boldsymbol{P}_{I,E,i} \\ -\boldsymbol{P}_{I,E,i} & \boldsymbol{P}_{R,E,i} \end{bmatrix} \quad \text{with} \quad \boldsymbol{P}_{E,i} \in \mathbb{R}^{2n\times 2n} \tag{2.12}$$

2.3 Adaptive Feedforward Algorithm

In order to couple virtual and experimental components, the parameter vector $\boldsymbol{\theta}$ has to be chosen such that the interface gap $\boldsymbol{e}$ is closed. In order to adapt $\boldsymbol{\theta}$ online, the use of a recursive least squares algorithm (see e.g. [11, 13]) is proposed, which minimizes the integral cost functional J defined in Eq. (2.13). Note that for the derivation of the adaption law, the above mentioned functions are used in their time discretized form. Here we use brackets to indicate a specific time instance. The cost functional includes a forgetting factor $\mu \in [0, 1]$, which enables a decreasing weighting of old values of $\boldsymbol{e}^T[i]\boldsymbol{e}[i]$ at ith time instances. The phase and gain matrices $\boldsymbol{P}_E$ and $\boldsymbol{P}_V$ as well as $\boldsymbol{P}_A$, which characterizes the actuator dynamics, are combined to $\boldsymbol{P}$.

$$\begin{aligned} J[k] &= \sum_{i=0}^{k} \mu^{k-i}\boldsymbol{e}^T[i]\boldsymbol{e}[i] \\ \text{with} \quad \boldsymbol{e}[i] &= \boldsymbol{y}_E[i] - \boldsymbol{y}_V[i] = \boldsymbol{W}[i]\underbrace{(\boldsymbol{P}_E - \boldsymbol{P}_V)\boldsymbol{P}_A}_{\boldsymbol{P}}\boldsymbol{\theta}[i] + \boldsymbol{W}[i]\underbrace{(\boldsymbol{\pi}_E[i] - \boldsymbol{\pi}_V[i])}_{\boldsymbol{\pi}[i]} \end{aligned} \tag{2.13}$$

Starting point for deriving the adaption law for the hybrid testing problem is the solution of the least squares problem, which is then rearranged as recursive algorithm:

$$\boldsymbol{0} = \frac{\partial J[k]}{\partial \boldsymbol{\theta}[k]} = \sum_{i=0}^{k} 2\mu^{k-i}\left(\boldsymbol{P}^T\boldsymbol{W}[i]^T\boldsymbol{W}[i]\boldsymbol{P}\boldsymbol{\theta}[k] + \boldsymbol{P}^T\boldsymbol{W}[i]^T\boldsymbol{W}[i]\boldsymbol{\pi}[i]\right) \tag{2.14}$$

$$\boldsymbol{\theta}[k] = \underbrace{\left(\sum_{i=0}^{k} \mu^{k-i}\boldsymbol{P}^T\boldsymbol{W}[i]^T\boldsymbol{W}[i]\boldsymbol{P}\right)^{-1}}_{\boldsymbol{R}[k]} \left(\sum_{i=0}^{k} -\mu^{k-i}\boldsymbol{P}^T\boldsymbol{W}[i]^T\boldsymbol{W}[i]\boldsymbol{\pi}[i]\right) \tag{2.15}$$

The solution of the least squares problem for the next time step $k + 1$ is arranged as follows:

$$\boldsymbol{\theta}[k+1] = \overbrace{\left(\sum_{i=0}^{k} \mu^{k+1-i}\boldsymbol{P}^T\boldsymbol{W}[i]^T\boldsymbol{W}[i]\boldsymbol{P} + \boldsymbol{P}^T\boldsymbol{W}[k+1]^T\boldsymbol{W}[k+1]\boldsymbol{P}\right)^{-1}}^{\boldsymbol{R}[k+1]} \cdot \left(\sum_{i=0}^{k} -\mu^{k+1-i}\boldsymbol{P}^T\boldsymbol{W}[i]^T\boldsymbol{W}[i]\boldsymbol{\pi}[i] - \boldsymbol{P}^T\boldsymbol{W}[k+1]^T\boldsymbol{W}[k+1]\boldsymbol{\pi}[k+1]\right)$$

Applying the Woodbury matrix identity allows to replace the inverse of the regressor matrix:

$$\boldsymbol{\theta}[k+1] = \overbrace{\left(\frac{1}{\mu}\boldsymbol{R}[k] - \frac{1}{\mu}\boldsymbol{R}[k]\boldsymbol{P}^T\boldsymbol{W}[k+1]^T\left(\boldsymbol{I} + \frac{1}{\mu}\boldsymbol{W}[k+1]\boldsymbol{P}\boldsymbol{R}[k]\boldsymbol{P}^T\boldsymbol{W}[k+1]^T\right)^{-1}\boldsymbol{W}[k+1]\boldsymbol{P}\boldsymbol{R}[k]\right)}^{\boldsymbol{R}[k+1]} \cdot \left(\sum_{i=0}^{k} -\mu\mu^{k-i}\boldsymbol{P}^T\boldsymbol{W}[i]^T\boldsymbol{W}[i]\boldsymbol{\pi}[i] - \boldsymbol{P}^T\boldsymbol{W}[k+1]^T\boldsymbol{W}[k+1]\boldsymbol{\pi}[k+1]\right)$$

Further simplification of the equations finally yields the recursive least squares adaption law:

$$\boldsymbol{\gamma}[k+1] = \frac{1}{\mu}(\boldsymbol{R}[k]\boldsymbol{P}^T\boldsymbol{W}[k+1]^T)(\boldsymbol{I} + \frac{1}{\mu}\boldsymbol{W}[k+1]\boldsymbol{P}\boldsymbol{R}[k]\boldsymbol{P}^T\boldsymbol{W}^T[k+1])^{-1} \tag{2.16}$$

$$\boldsymbol{\theta}[k+1] = \boldsymbol{\theta}[k] + \boldsymbol{\gamma}[k+1]\underbrace{(\boldsymbol{W}[k+1]\boldsymbol{P}\boldsymbol{\theta}[k] + \boldsymbol{W}[k+1]\boldsymbol{\pi}[k+1])}_{\boldsymbol{e}'[k+1]} \tag{2.17}$$

$$\boldsymbol{R}[k+1] = \frac{1}{\mu}(\boldsymbol{R}[k] - \boldsymbol{\gamma}[k+1]\boldsymbol{W}[k+1]\boldsymbol{P}\boldsymbol{R}[k]) \tag{2.18}$$

Note that $\boldsymbol{e}'$ is the a-priori gap, which can be measured, whereas $\boldsymbol{e}$ is the a-posteriori interface gap, which is used in the cost functional J. The RLS algorithm allows the practical application of adaptive feedforward compensation in Real Time Hybrid Testing with multiple DoF interfaces as a single forgetting factor μ has to be chosen. Note that the phase and gain matrix $\boldsymbol{P}$ characterizing plant dynamics are used in the adaption law. $\boldsymbol{P}$ can be identified prior to the adaption process by exciting each actuation DoF separately or with uncorrelated noise.

2.4 Numerical Case Study

The algorithm is applied to a simple lumped mass problem with a two DoF interface. The arrangement of the masses is illustrated in Fig. 2.4. The mass and stiffness parameters are given in Table 2.1. Proportional damping with a stiffness proportional coefficient $\alpha = 0.01$ and a mass proportional coefficient $\beta = 0.001$ is used, which confers a modal damping of 0.5 % to the submodels. The models and the interface synchronization control were implemented in Matlab$^{\text{ő}}$ Simulink$^{\text{ő}}$. The excitation force $f_{V,ext} = \sum_{i=1}^{4} = A_i \sin \omega_i t$ was applied on mass 1. The excitation frequencies were $\omega_1 = 20\frac{1}{\text{rad}}$, $\omega_2 = 30\frac{1}{\text{rad}}$, $\omega_3 = 50\frac{1}{\text{rad}}$ and $\omega_4 = 60\frac{1}{\text{rad}}$. The amplitudes $A_1 = 4\,\text{N}, A_2 = 10\,\text{N}, A_3 = 10\,\text{N}$ and $A_4 = 20\,\text{N}$. The forgetting factor for the RLS algorithm was chosen as $\mu = 0.99$ The identification was running for 10 s with an excitation of 5 s on each actuation DoF. The adaption with the RLS algorithm starts at $t = 10\,\text{s}$.

Figures 2.5 and 2.6 show the interface synchronization for both interface DoF. In the investigated case the algorithm adapts within 2 s and is then accurately ensuring compatibility. The adaption time is depending on the properties of the coupled components. Figure 2.7 shows the comparison of the displacement of mass 4 with the reference overall system. After the adaption process the reference system is simulated accurately. In all of our numerical studies the algorithm was found to be very robust. As indicated by Fig. 2.8 noisy force and displacement signals have little impact on adaption time and stability issues in this numerical case study which indicates a good feasibility for practical implementation.

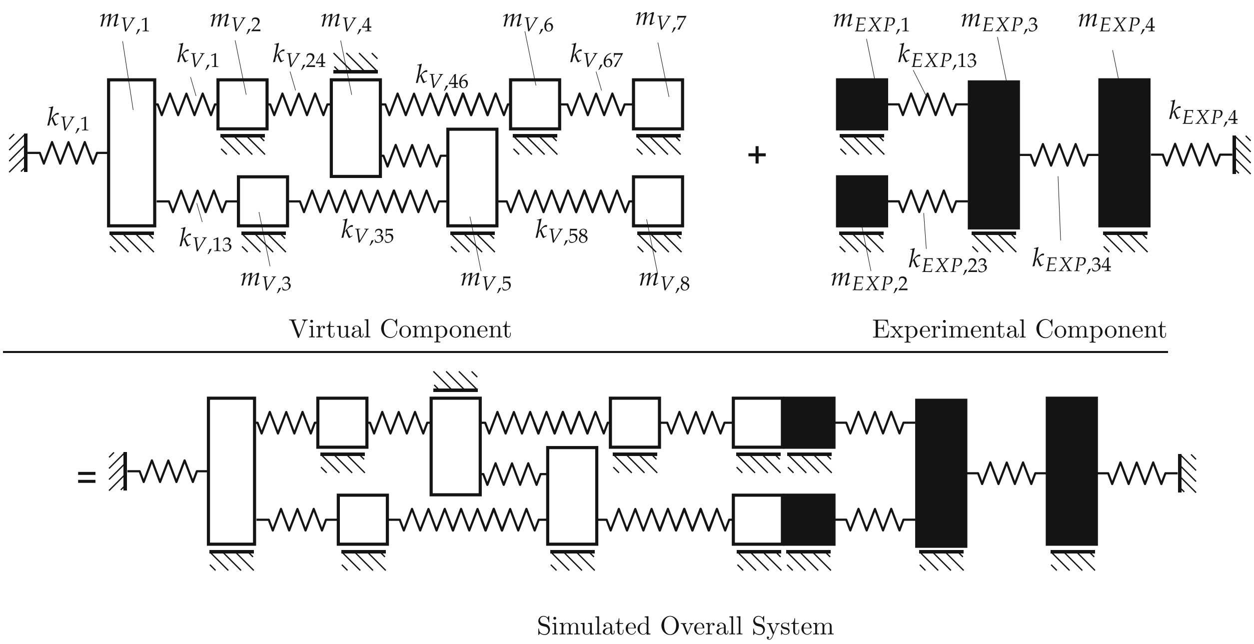

Fig. 2.4 Arrangement of the lumped mass system used for numerical studies

Table 2.1 System parameters used in the numerical case study

Virtual component (V)			
Stiffness (N/m)		Mass (kg)	
$k_{V,1}$	25,000,000	$m_{V,1}$	10
$k_{V,12}$	10,000,000	$m_{V,2}$	3
$k_{V,13}$	10,000,000	$m_{V,3}$	3
$k_{V,24}$	10,000,000	$m_{V,4}$	3
$k_{V,35}$	10,000,000	$m_{V,5}$	3
$k_{V,45}$	10,000,000	$m_{V,6}$	2
$k_{V,58}$	500,000	$m_{V,7}$	2
$k_{V,46}$	20,000,000	$m_{V,8}$	4
$k_{V,67}$	20,000,000		
Test specimen (EXP)			
Stiffness (N/m)		Mass (kg)	
$k_{EXP,13}$	2,500,000	$m_{EXP,1}$	2
$k_{EXP,23}$	2,000,000	$m_{EXP,2}$	4
$k_{EXP,34}$	10,000,000	$m_{EXP,3}$	8
$k_{EXP,4}$	10,000,000	$m_{EXP,4}$	5

2.5 Conclusion

In this paper we propose an adaptive feedforward technique with harmonic regressor for interface synchronization in Real Time Hybrid Testing. The approach makes use of the assumption of harmonic excitation and steady state. It addresses stability and accuracy issues in cases where the simulated overall system is a structural system with low damping. Multiple DoF interfaces are necessary in many applications. As the choice of adaption gain parameters is getting a complex task for tests with multiple DoF interfaces, we propose the use of a recursive least square algorithm for the adaption of the harmonic parameters with only a single parameter for the controller design. Future work will include the experimental validation on a test rig with a multiple DoF interface as well as the comparison with other interface synchronization techniques for Real Time Hybrid Testing.

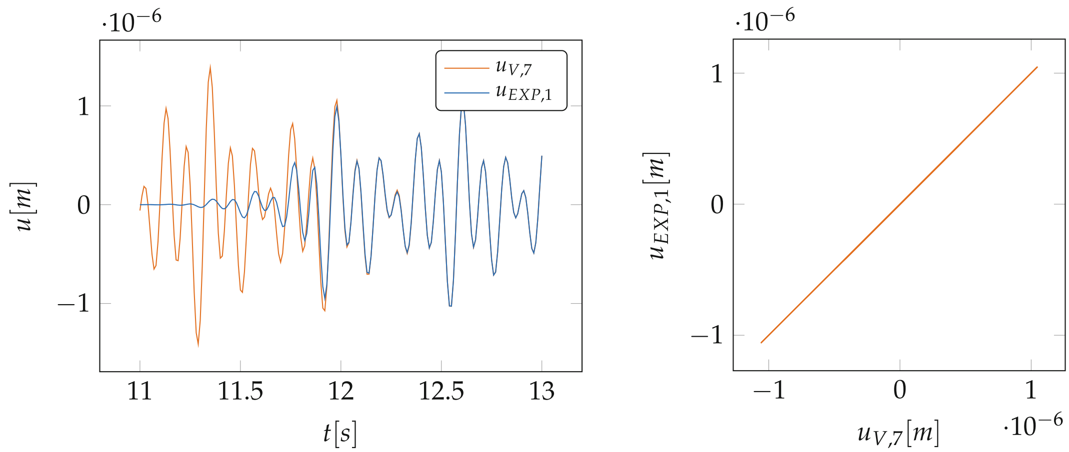

Fig. 2.5 Interface synchronization for the first interface DoF: the *left hand figure* shows the adaption process, the *right hand figure* shows the synchronization in the adapted state

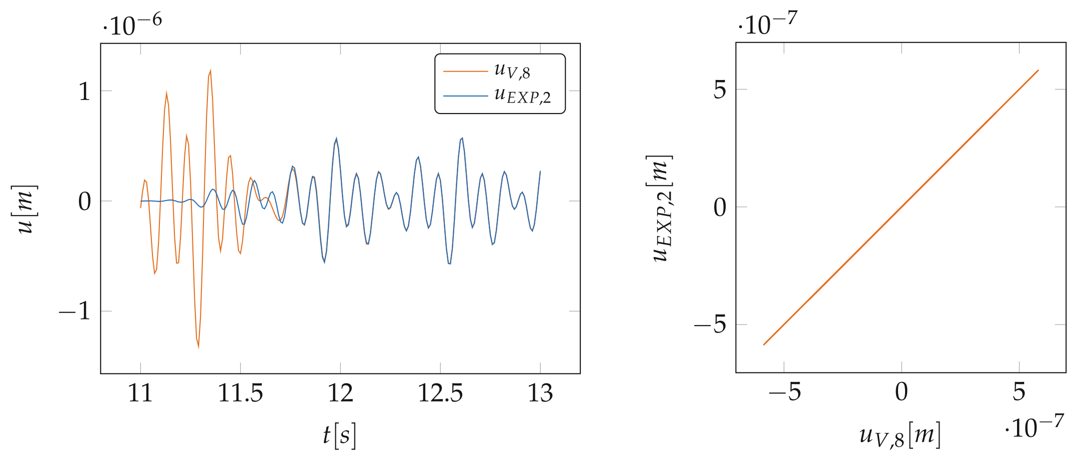

Fig. 2.6 Interface synchronization for the second interface DoF: the *left hand figure* shows the adaption process, the *right hand figure* shows the synchronization in the adapted state

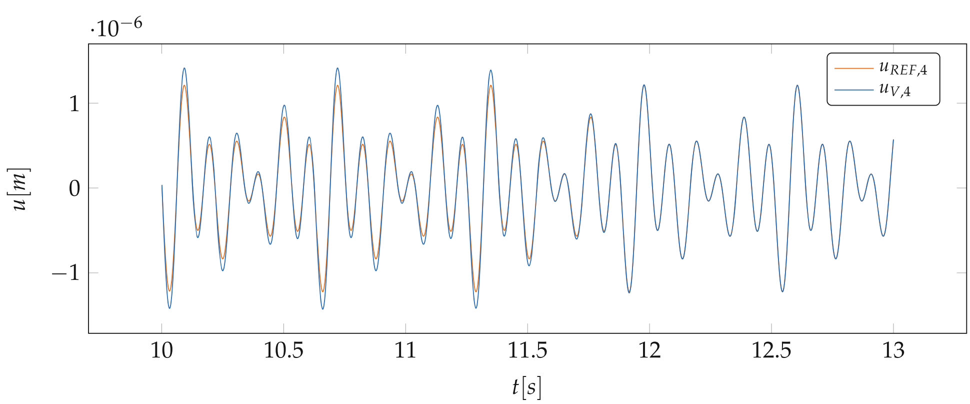

Fig. 2.7 Displacement of mass 4 during the adaption process compared with the reference overall system

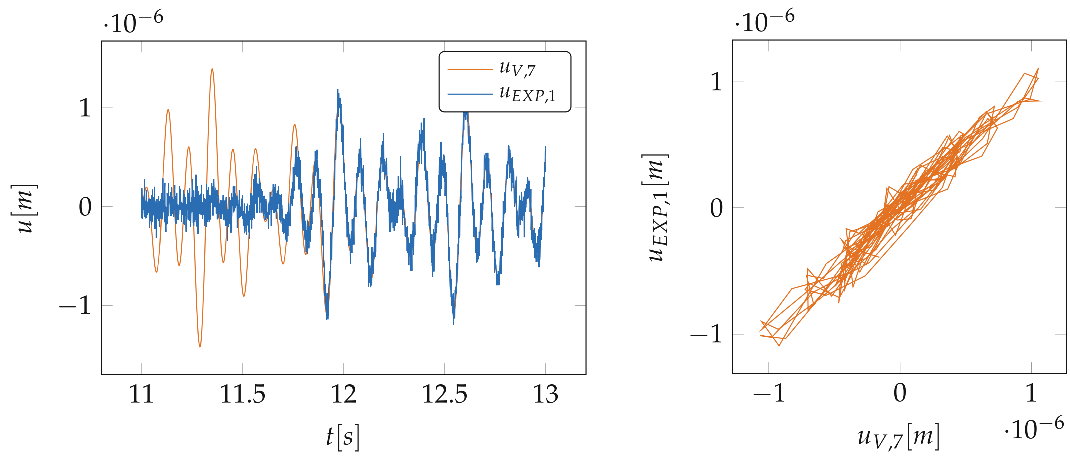

Fig. 2.8 Interface synchronization for the first interface DoF with added noise on force and displacement signals: the *left hand figure* shows the adaption process, the *right hand figure* the synchronization in the adapted state

References

1. Bartl, A., Mayet, J., Rixen, D.J.: Adaptive feedforward compensation for real time hybrid testing with harmonic exciation. In: Proceedings of the 11th International Conference on Engineering Vibration, Sept 2015
2. Bayard, D.S.: A general theory of linear time-invariant adaptive feedforward systems with harmonic regressors. IEEE Trans. Autom. Control **45**(11), 1983–1996 (2000)
3. Blakeborough, A., Darby, A., Williams, M.: The development substructure of real-time testing. Philos. Trans. Math. Phys. Eng. Sci. **359**(1786), 1869–1891 (2001)
4. Bodson, M., Sacks, A., Khosla, P.: Harmonic generation in adaptive feedforward cancellation schemes. IEEE Trans. Autom. Control **39**(9), 1939–1944 (1994)
5. Bonnet, P.A.: The development of multi-axis real-time substructure testing. Ph.D. thesis (2006)
6. Bosse, D., Radner, D., Schelenz, R., Jacobs, G.: Analysis and application of hardware in the loop wind loads for full scale Nacelle ground testing. DEWI Mag. **43**, 65–70 (2013)
7. Botelho, R.M., Christenson, R.E.: Mathematical equivalence between dynamic substructuring and feedback control theory. In: Proceedings of the 33rd IMAC (2015)
8. Darby, A.P., Williams, M.S., Blakeborough, A.: Stability and delay compensation for real-time substructure testing. J. Eng. Mech. **128**, 1276–1284 (2002)
9. De Klerk, D., Rixen, D.J., Voormeeren, S.N.: General framework for dynamic substructuring: history, review and classification of techniques. AIAA J. **46**(5), 1169–1181 (2008)
10. Glover, J.: Adaptive noise canceling applied to sinusoidal interferences. IEEE Trans. Acoust. Speech Signal Process. **25**, 484–491 (1977)
11. Haykin, S.: Adaptive Filter Theory. Upper Saddle River, Prentice Hall (2010)
12. Horiuchi, T., Inoue, M., Konno, T., Namita, Y.: Real-time hybrid experimental system with actuator delay compensation and its application to a piping system with energy absorber. Earthq. Eng. Struct. Dyn. **28**(10), 1121–1141 (1999)
13. Ioannou, P., Sun, J.: Robust Adaptive Control. Dover Publications, New York (2013)
14. Jungblut, T., Wolter, S., Matthias, M., Hanselka, H.: Using numerical models to complement experimental setups by means of active control of mobility. Appl. Mech. Mater. **70**, 357–362 (2011)
15. Li, G.: A generic dynamically substructured system framework and its dual counterparts, pp. 10101–10106 (2014)
16. Li, G., Na, J., Stoten, D.P., Ren, X.: Adaptive neural network feedforward control for dynamically substructured systems. IEEE Trans. Control Syst. Technol. **22**(3), 944–954 (2014)
17. Nakashima, M., Kato, H., Takaoka, E.: Development of real-time pseudo dynamic testing. Earthq. Eng. Struct. Dyn. **21**, 79–92 (1992)
18. Plummer, A.: Model-in-the-loop testing. Proc. Inst. Mech. Eng. I: J. Syst. Control Eng. **220**, 183–199 (2006)
19. Stoten, D., Hyde, R.: Adaptive control of dynamically substructured systems: the single-input single-output case. Proc. Inst. Mech. Eng. I: J. Syst. Control Eng. **220**(2), 63–79 (2006)
20. Stoten, D., Li, G., Tu, J.: Model predictive control of dynamically substructured systems with application to a servohydraulically actuated mechanical plant. IET Control Theory Appl. **4**(2), 253–264 (2010)
21. Stoten, D., Tu, J., Li, G.: Synthesis and control of generalized dynamically substructured systems. Syst. Control Eng. **223**, 371–392 (2010)
22. Tu, J.: Development of numerical-substructure-based and output-based substructuring controllers. In: Structural Control and Health Monitoring, June 2012, pp. 918–936. Wiley, New York (2013)
23. Wagg, D.J., Stoten, D.P.: Substructuring of dynamical systems via the adaptive minimal control synthesis algorithm. Earthq. Eng. Struct. Dyn. **30**(6), 865–877 (2001)
24. Wallace, M.I., Wagg, D.J., Neild, S.a.: An adaptive polynomial based forward prediction algorithm for multi-actuator real-time dynamic substructuring. Proc. R. Soc. A Math. Phys. Eng. Sci. **461**(2064), 3807–3826 (2005)

Chapter 3
Controls Based Hybrid Sub-Structuring Approach to Transfer Path Analysis

Joseph A. Franco, Rui M. Botelho, and Richard E. Christenson

Abstract In the design of mechanical systems, there are constraints imposed on the vibration of mechanical equipment to limit the vibration transmission into its support structure. To accurately predict the coupled system response, it is important to capture the coupled interaction of the two portions, i.e., the mechanical equipment and the support structure, of the mechanical system. Typically during a design, the analysis of the full mechanical system is not possible because a large part of the system may be non-existent. Existing methods known as Transfer Path Analysis and Frequency Based Substructuring are techniques for predicting the coupled response of vibrating mechanical systems. In this paper, a control based hybrid substructuring approach to Transfer Path Analysis is proposed. By recognizing the similarities between feedback control and dynamic substructuring, this paper demonstrates that this approach can accurately predict the coupled dynamic system response of multiple substructured systems including operating mechanical equipment with a complex vibration source. The main advantage of this method is that it uses blocked force measurements in the form of a power spectral density matrix measured uncoupled from the rest of the system. This substructuring method is demonstrated using a simplified case study comprised of a two-stage vibration isolation system and excited by operating mechanical equipment.

Keywords Transfer path analysis • Frequency based substructuring • Hybrid substructuring • Feedback control • System level vibration analysis

3.1 Introduction

Vibration of mechanical equipment can result in fatigue, detection, and/or environmental concerns for a structural system. A critical aspect of the design of systems that include mechanical equipment is quantifying the level of transmitted vibration energy through the supporting structure. The system design typically consists of strict constraints imposed on the vibration transmission of the mechanical equipment through the support structure. During the design phase of a system, the mechanical equipment is pre-existing either from previous designs or they are commercially available components purchased from a vendor. The support structure is typically non-existent and is designed and optimized using Computer Aided Design (CAD) software. This makes testing of the full mechanical system, impossible. For these reasons, the analysis of the mechanical system normally requires the combination of multiple quantifications of dynamics of various substructures of the mechanical system.

Existing methods known as Transfer Path Analysis (TPA) are frequency response functions (FRF) based techniques that describe the dynamics of the mechanical system by the multiplication of the FRFs of the system substructures. This method can also be used to combine theoretical (FEM) models and experimental measurements of system substructures. Some of these methods were developed by Plunt [1, 2] for the automotive industry and Darby [3] for the marine industry. However, the disadvantage of these TPA methods is that they do not always consider the dynamic coupling between the receiving and exciting substructures. This limitation becomes critical at low frequencies due to the interaction between the modes of the individual substructures.

Variations of TPA methods are known as Frequency Based Substructuring (FBS) methods which allow for the calculation of the entire mechanical system dynamic response based on the FRFs of the system substructures using various methods. Primary developments of FBS methods are Crowley et al. [4], Jetmundsen et al. [5], Imregun and Robb [6] and later on Gordis [7] and de Klerk [8]. Generally, this work demonstrated a wide variety of methods to couple substructures based on

J.A. Franco (✉) • R.M. Botelho • R.E. Christenson
Department of Civil and Environmental Engineering, University of Connecticut, 261 Glenbrook Road Unit 3037, Storrs, CT 06269-3037, USA
e-mail: joseph.franco@uconn.edu

M. Allen et al. (eds.), *Dynamics of Coupled Structures, Volume 4*, Conference Proceedings of the Society for Experimental Mechanics Series, DOI 10.1007/978-3-319-29763-7_3

either numerically computed or experimentally measured FRFs. However, a large drawback of these methods is that they generally require that the vibratory excitation be known and be able to be quantified; de Klerk [9] did significant work to develop methods to identify and quantify these excitation sources. However, this can be fairly difficult and labor intensive in a real life experimental environment.

Real-time hybrid substructuring (RTHS) is a relatively new test method, recently made more practical because of advances in computer power, digital signal processing hardware/software, and hydraulic control hardware that is used for vibration testing for calculating the dynamic performance of a mechanical system by partitioning a mechanical system into physical and numerical substructures and then interfacing them together in real-time similar to hardware-in-the-loop testing. Early developments of RTHS include Horiuchi et al. [10], Nakashima and Masaoka [11], and Darby et al. [12]. As in FBS methods, RTHS is also a hybrid method, which takes advantage of both experimental methods along with numerical computational methods of system substructures. This method allows the dynamic excitation of the system to be unknown since it is represented in the physical substructure. However, this system is highly dependent on the performance of the actuator system that is used to transmit the displacement feedback from the numerical substructure to the physical substructure. For low frequencies, this is typically a hydraulic system which can be difficult to get accurate reference tracking performance.

In this paper, a practical control based hybrid experimental-numerical approach referred to Transfer Path Hybrid Substructuring (TPHS) is proposed. This approach was developed out of recognition of the similarities of techniques in both the feedback control and the dynamic substructuring fields. Botelho [13] provides an excellent comparison of the mathematically similar formulations for both feedback control theory and dynamic substructuring. By identifying these similarities, it allows the leveraging of elementary feedback control theory, to the Transfer Path Analysis and Frequency Based Substructuring fields. This paper, leverages these similarities in order demonstrates that this new TPHS method can be used to accurately predict the coupled dynamics of multiple substructures of a mechanical system. This method is also a hybrid approach which allows for each of the system substructures to be represented by either experimentally obtained or numerically computed FRFs. This paper will demonstrate in a simplified case study how a power spectral density (PSD) matrix can be used as input to the substructuring procedure.

3.2 Real Time Hybrid Substructuring

Real Time Hybrid Substructuring (RTHS) is a test method that provides the capability to isolate and physically test the more advanced critical mechanical equipment of a mechanical system at the design phase of the system while including the dynamic interaction with a numerical representation of the remainder of the support structure. This is advantageous over more traditional substructuring techniques because the portion of the system that makes up the physical substructure is not required to be dynamically quantified. A typical RTHS test is made up of the numerical substructure, the physical substructure as well as the actuator system required to command calculated displacements from the numeric substructure to the physical substructure. Figure 3.1 shows this typical RTHS test layout displayed as a control based block diagram.

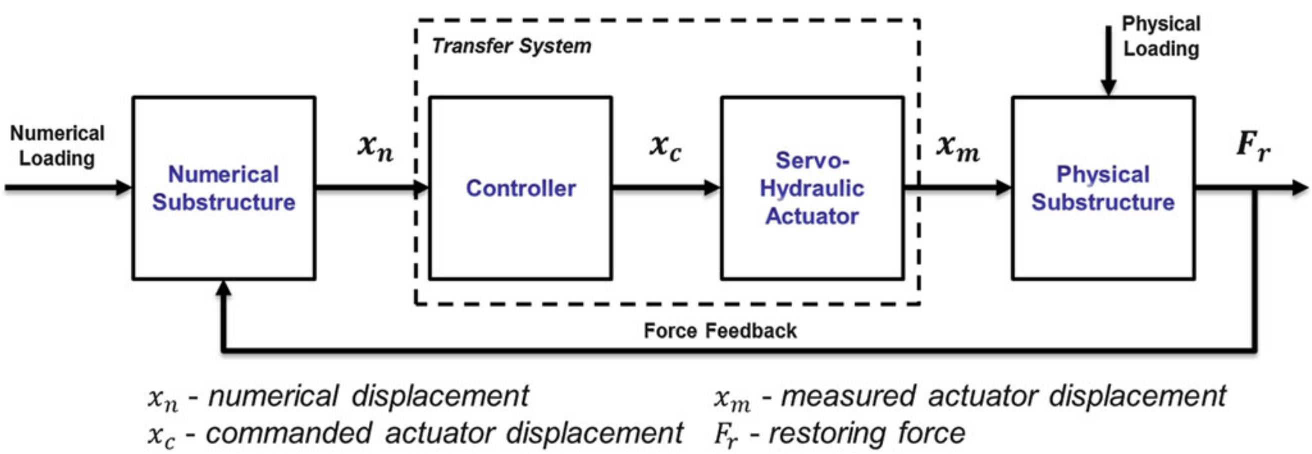

Fig. 3.1 Control block diagram of a typical RTHS test

The main disadvantage of RTHS is the dependence on this transfer system's dynamics. At low frequencies, where dynamic coupling of system substructures is necessary, this transfer system is typically a servo-hydraulic actuator system. Servo-hydraulic actuator systems tend to have significant frequency dependent magnitude attenuation and time delay. A large portion of the research done concerning RTHS is compensating and controlling these frequency dependent dynamics.

The mechanical system of interest in this paper is that which consists of mechanical equipment, which is the vibration source, and its support structure. The mechanical portion of the system lends itself well to the physical substructure of the RTHS layout. This mechanical equipment typically have complex dynamics and acoustic excitations which are difficult to model with classic numerical methods also possibility because of non-linarites and time-variant properties of the mechanical equipment. The support structure, on the other hand, lends itself well to the numerical substructure of the RTHS layout shown in Fig. 3.1. This paper's interest is the system excitation source's that come from the mechanical component, i.e., the physical substructure and is not interested in vibratory excitations that come from the support structure, i.e., the numerical substructure. Therefore, the numerical loading shown in Fig. 3.1 will be ignored for this paper.

The physical loading shown in Fig. 3.1 is analogous to what is known in the controls field as a system disturbance. In this case, the disturbance is the excitation of the physical substructure and it is the interest of this paper to quantify how that excitation affects the system dynamics as well as how the excitation is transmitted through the system. Spite the difference in the desired outcome of the analysis, controls based analysis methods and tools can be leveraged to analyze the system.

3.3 Controls Approach to Transfer Path Hybrid Substructuring

This paper attempts to use the RTHS control diagram shown in Fig. 3.1 and simple control diagram analysis to develop a new approach to substructuring referred to Transfer Path Hybrid Substructuring (TPHS). From the block diagram shown in Fig 3.1 (not including the numerical loading), the equation for the closed loop control diagram is given by

$$F_r = -PANF_r + P_i \tag{3.1}$$

Where P is the physical substructure, N is the numeric substructure, A is the transfer system, and P_i is the excitation load on the system, referred to here as the physical loading. Rearranging Equation (3.1) in terms of the reactant force, F_r gives the fundamental equation of TPHS shown below

$$F_r = \left[\frac{1}{1 + PAN}\right] P_i \tag{3.2}$$

This simple equation gives the formula for solving for the coupled reactant force of the numerical and physical substructures at the interaction points between the two substructures.

One portion of the control diagram shown in Fig 3.1 that is not necessary with this method is the actuator dynamics transfer function. Specifically, when the physical substructure is tested, the input signals to the FRF calculations either could be x_c, or the measured displacements, x_m. If x_c is used as the physical substructure input signals, then the measured transfer function will include the actuator transfer function which is the quantification of the transmission of the x_c, to the actual x_m, of the actuators. With servo-hydraulic actuators this can be a significant level of frequency dependent magnitude attenuation in addition to frequency dependent time delay. However, if x_m is used as the physical substructure input signal, then the measured transfer function does not include these additional actuator dynamics and the measured performance of the physical substructure is calculated in terms of a normalized input. If it is assumed that we have perfect actuator tracking, i.e., x_m is equal to x_c, then the numerical and physical substructures have like terms and can be multiplied together and the A transfer function can be removed from Eq. (3.2). This is a significant advantage of this method over RTHS. A large portion of the complication of RTHS is compensating for the frequency dependent actuator dynamics which can be substantial. TPHS bypasses this complication by assuming ideal actuator reference tracking. This simplifies the governing equation of TPHS even further to

$$F_r = [I + PN]^{-1} P_i \tag{3.3}$$

Equation (3.3) calculates the coupled reactant forces at the interaction points between the two substructures; however, this is not the metric of interest. To calculate the force at the base of the full system, the reactant force is then multiplied by a force

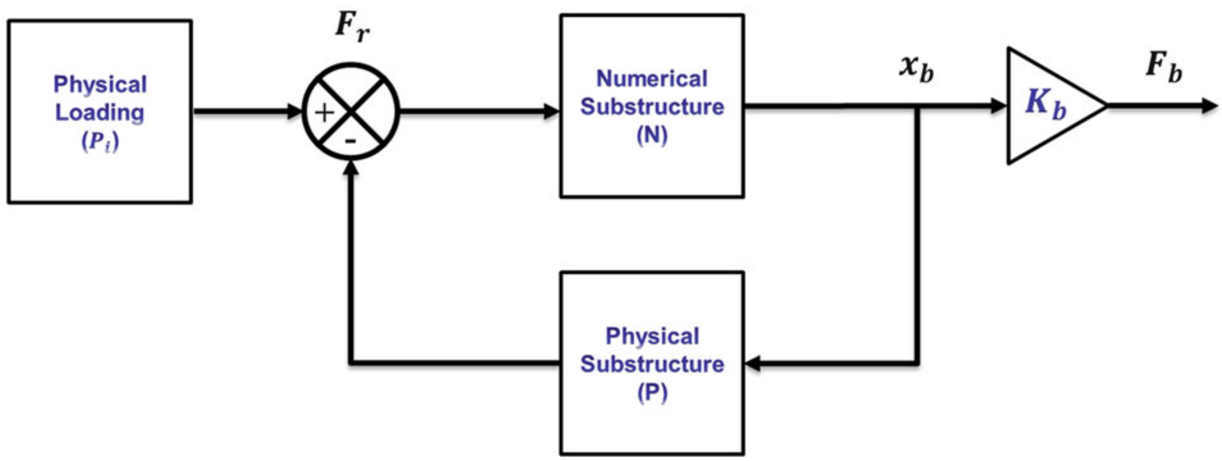

Fig. 3.2 Control diagram representing the TPHS method

transmissibility transfer function which is equal to the numeric substructure multiplied by the base isolator stiffness, K_bN. The TPHS equation for the base forces of the full system is

$$F_b = K_bN[I + PN]^{-1}P_i \tag{3.4}$$

where F_b is the force at the base of the full system. Figure 3.2 shows Eq. (3.4) as a simple feedback control diagram.

Figure 3.2 shows that the critical part of this analysis method is the feedback loop. Without it, the open-loop solutions is given by

$$F_b = K_bNP_i \tag{3.5}$$

and by comparing this to Eq. (3.4), it is shown that this critical feedback loop is represented by the $[I + PN]^{-1}$ term. The difference between the closed-loop and open-loop analysis will be investigated further later on.

3.3.1 Physical Loading Using Auto Power Spectral Densities

In most cases, mechanical systems have many complex excitations and it may be very difficult to quantify them. Therefore, mechanical equipment vibration is typically quantified in power spectral densities (PSD). This is a main disadvantage of most transfer path and frequency base substructuring methods; the source of the dynamics is needed in order to experimentally measure transfer functions of the physical substructure used in these hybrid methods.

This is the main advantage of Transfer Path Hybrid Substructuring. The controls based approach allows the physical excitation of the system to be in the form of a PSD (or a PSD matrix for the MDOF case). In the case of MDOF, the power spectral density matrix consists of auto power spectral densities along the diagonal of the matrix and cross power spectral densities in the off-diagonal terms between the two respective signals. The form of this PSD matrix is given below

$$\boldsymbol{G_{p_ip_i}} = \begin{bmatrix} G_{11} & G_{12} & \cdots & G_{1n} \\ G_{21} & G_{22} & \cdots & G_{2n} \\ \vdots & \vdots & \ddots & \vdots \\ G_{n1} & G_{n2} & \cdots & G_{nn} \end{bmatrix} \tag{3.6}$$

Where $\boldsymbol{G_{p_ip_i}}$ is the PSD matrix of the physical loading and n is the number of signal locations. The diagonal terms, G_{11}, G_{22}, … G_{nn} are the auto power spectral densities while all other off diagonal terms, G_{12}, G_{21}, … terms are the cross power spectral densities.

3.4 Numeric Example

In order to demonstrate this method numerically, each of the substructures, as well as the physical loading, must be quantified. One complication of quantifying each of these quantities is that they are frequency dependent. The simplest solution to this issue is to use Laplace domain or s-domain transfer functions to represent the frequency dependent response of the substructures. The following is a simplified example of this approach.

The numeric substructure, as shown in Fig. 3.2, has a force input and a displacement output. In dynamics, this is known as flexibility. The equation for the system flexibility is derived starting with the equation of motion

$$\left[Ms^2 + Cs + K\right]x = F \tag{3.7}$$

where M, C and K are the substructures' mass, damping and stiffness properties, F is the excitation force, x is the system displacement and s is the Laplace constant. The flexibility equation of the numerical substructure, in the s-domain, is then derived by rearranging Equation (3.7) into

$$\frac{x}{F} = \frac{1}{Ms^2 + Cs + K} \tag{3.8}$$

The physical substructure, as shown in Fig. 3.2 has an input base displacement and a resultant base force. This transfer function is derived using the following rigid body diagram shown in Fig. 3.3.

where F_b is the reactant force at the base due to the input base displacement, x_b. The characteristic equation of motion of this system is Eq. (3.7) where the input force is calculated by

$$[Cs + K]\,x_b = F \tag{3.9}$$

Therefore, the equation of motion becomes

$$[Cs + K]\,x_b = \left[Ms^2 + Cs + K\right]x \tag{3.10}$$

Rearranging this equation to solve for the system displacement due to base input displacement gives

$$\frac{x}{x_b} = \frac{Cs + K}{Ms^2 + Cs + K} \tag{3.11}$$

Using Eq. (3.11) in the equation for the reactant force of the spring-damper shown below

$$F_b = [Cs + K]\,(x_b - x) \tag{3.12}$$

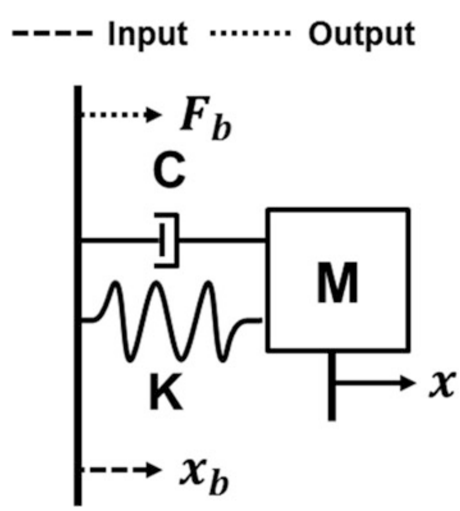

Fig. 3.3 Rigid body diagram of a single DOF system with a base displacement input

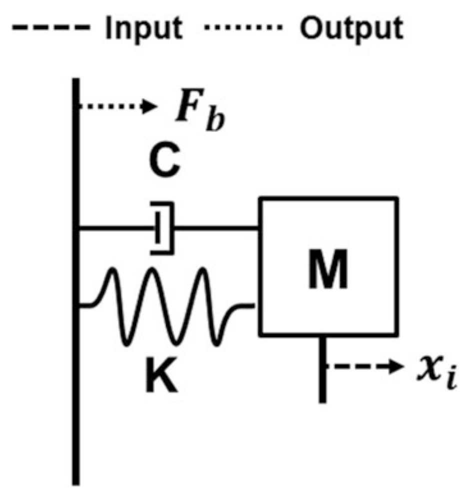

Fig. 3.4 Rigid body diagram of a single DOF system with a displacement input

gives the s-domain transfer function for the physical substructure

$$\frac{F_b}{x_b} = [Cs + K]\left(1 - \frac{Cs + K}{Ms^2 + Cs + K}\right) \tag{3.13}$$

This is the equation for the reactant base force due to a base displacement excitation, also sometimes known as dynamics stiffness.

Lastly, the physical loading needs to be realized using s-domain transfer functions. For this simple example it is assumed that the physical loading is a commanded displacement excitation. The transfer function of the physical loading is reactant force due to an input displacement excitation. This transfer function is derived using a rigid body diagram shown in Fig. 3.4.

where x_i is the input displacement. The characteristic equation of motion of this system is Eq. (3.7) where the input force is calculated by

$$Ms^2x_i = F \tag{3.14}$$

Therefore, the equation of motion becomes

$$\left[Ms^2 + Cs + K\right]\{x\} = Ms^2x_i \tag{3.15}$$

Rearranging this equation to solve for the system displacement due to base input displacement gives

$$\frac{x}{x_i} = \frac{Ms^2}{Ms^2 + Cs + K} \tag{3.16}$$

From this equation, to get the reactant forces, we multiply by the characteristic equation of the system's spring/damper shown in

$$\frac{F_b}{x_i} = (Cs + K)\frac{Ms^2}{Ms^2 + Cs + K} \tag{3.17}$$

In order to verify that TPHS is an accurate method, it was compared to the traditional dynamic substructuring approach to solve a simple uni-axial two DOF system. Figure 3.5 shows a diagram of this example two DOF uni-axial system.

For this example the displacement excitation is applied to M_1 and both the TPHS and traditional dynamic substructuring is used to solve for the reactant force at the connection between the two substructures similar to what is shown in Fig. 3.2. The equations of motion of this system are given by the following system of equations.

$$\begin{Bmatrix} F_1 \\ F_2 \end{Bmatrix} = \left[\boldsymbol{M}s^2 + \boldsymbol{C}s + \boldsymbol{K}\right]\begin{Bmatrix} x_1 \\ x_2 \end{Bmatrix} \tag{3.18}$$

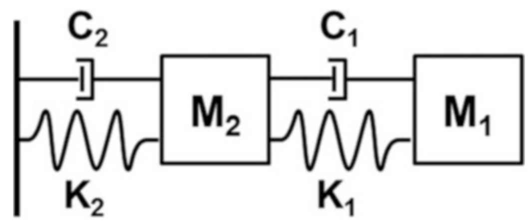

Fig. 3.5 Diagram of example two DOF uni-axial system

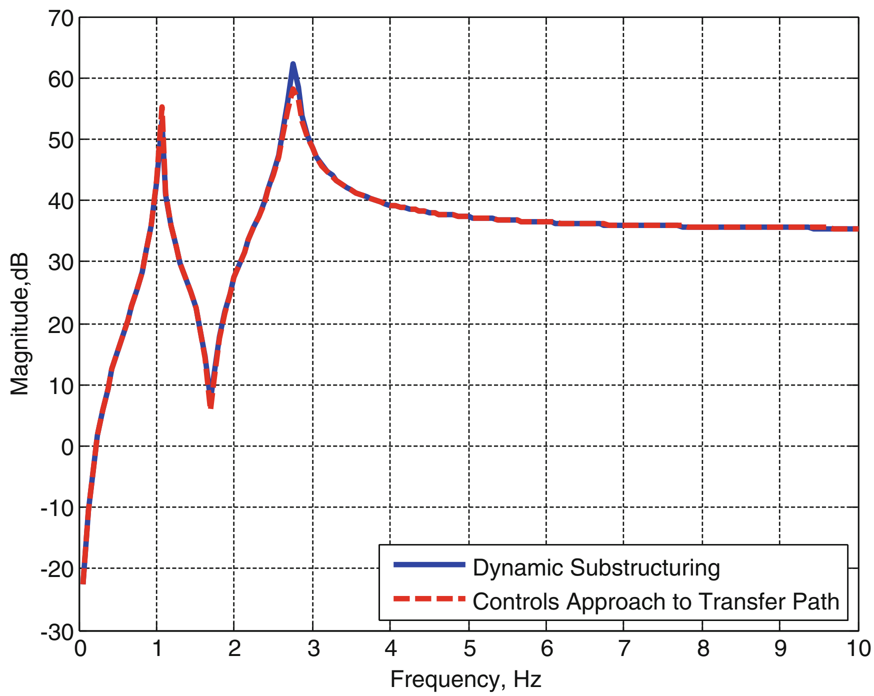

Fig. 3.6 Comparison of dynamic substructuring vs. transfer path hybrid substructuring

where

$$\boldsymbol{M} = \begin{bmatrix} M_1 & 0 \\ 0 & M_2 \end{bmatrix} \tag{3.19}$$

$$\boldsymbol{C} = \begin{bmatrix} C_1 & -C_1 \\ -C_1 & C_1 + C_2 \end{bmatrix} \tag{3.20}$$

$$\boldsymbol{K} = \begin{bmatrix} K_1 & -K_1 \\ -K_1 & K_1 + K_2 \end{bmatrix} \tag{3.21}$$

The same equation for reactant force due to displacement excitation shown in Eq. (3.17) can be applied here but replacing the SDOF scalars with MDOF matrices.

$$\frac{\{F_r\}}{\{x_i\}} = (\boldsymbol{C}s + \boldsymbol{K}) \cdot \boldsymbol{M}s^2\left[\boldsymbol{M}s^2 + \boldsymbol{C}s + \boldsymbol{K}\right]^{-1} \tag{3.22}$$

The results from Eq. (3.22) and the results from the TPHS using Eq. (3.2) are compared in Fig 3.6.

These results show that the TPHS method can accurately substructure two substructures together in the same manner as dynamic substructuring. This example shows that the fundamental theory of TPHS is equivalent to the more traditional method of dynamic substructuring.